JOC The Journal of Organic Chemistry

Article

pubs.acs.org/joc

Octazethrene and Its Isomer with Different Diradical Characters and Chemical Reactivity: The Role of the Bridge Structure

Pan Hu,[†] Sangsu Lee,[‡] Kyu Hyung Park,[‡] Soumyajit Das,[†] Tun Seng Herng,[§] Théo P. Gonçalves,[∥] Kuo-Wei Huang,[∥] Jun Ding,*[,§] Dongho Kim,*[,‡] and Jishan Wu*[,†]

[†]Department of Chemistry, National University of Singapore, 3 Science Drive 3, 117543 Singapore

[‡]Spectroscopy Laboratory for Functional π-Electronic Systems and Department of Chemistry, Yonsei University, Seoul 120-749, Korea

[§]Department of Materials Science & Engineering, National University of Singapore, 119260 Singapore

[∥]Division of Physical Science and Engineering and KAUST Catalysis Center, King Abdullah University of Science and Technology (KAUST), Thuwal 23955-6900, Kingdom of Saudi Arabia

Supporting Information

ABSTRACT: The fundamental relationship between structure and diradical character is important for the development of open-shell diradicaloid-based materials. In this work, we synthesized two structural isomers bearing a 2,6-naphthoquinodimethane or a 1,5-naphthoquinodimethane bridge and demonstrated that their diradical characters and chemical reactivity are quite different. The mesityl-or pentafluorophenyl-substituted octazethrene derivatives **OZ-M**/**OZ-F** and their isomer **OZI-M** (with mesityl substituents) were synthesized via an intramolecular Friedel−Crafts alkylation followed by oxidative dehydrogenation strategy from the key building blocks **4** and **11**. Our detailed experimental and theoretical studies showed that both isomers have an open-shell singlet ground state with a remarkable diradical character (y_0 = 0.35 and 0.34 for **OZ-M** and **OZ-F**, and y_0 = 0.58 for **OZI-M**). Compounds **OZ-M** and **OZ-F** have good stability in an ambient environment, while **OZI-M** has high reactivity and can be easily oxidized to a dioxo product **15**, which can be correlated to their different diradical characters. Additionally, we investigated the physical properties of **OZ-M**, **OZ-F**, and **15**.

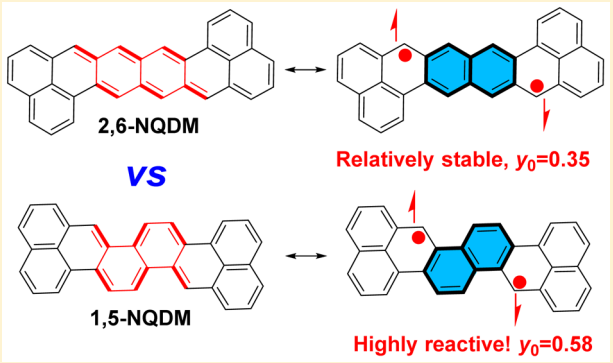

INTRODUCTION

Open-shell π-conjugated polycyclic hydrocarbons (PHs) have recently attracted tremendous interest due to their unique electronic, optical and magnetic properties applicable to organic electronics, nonlinear optics, spintronics, and energy storage devices.[1] So far, thanks to the development of efficient stabilizing strategies and synthetic methods, several types of stable open-shell PHs with a singlet diradical ground state have been reported, which include indenofluorenes,[2] bisphenalenyls,[3] zethrenes,[4] anthenes,[5] and quinoidal rylenes.[6] Most of the reported open-shell molecules contain a pro-aromatic quinodimethane (QDM), naphthoquinodimethane (NQDM), or anthraquinodimethane (AQDM) substructure, which can recover their aromaticity in the diradical form and serve as the major driving force to be a diradical in the ground state. Recently, there has been increased interest in studying the chemical and physical properties of different structural isomers. For example, Tobe and Haley et al. reported several indenofluorene isomers by embedding three types of QDM units (*p*-QDM, *o*-QDM, and *m*-QDM) in the aromatic hydrocarbon framework (Figure 1a).[2a,b,f] Interestingly, the diradical characters and the reactivity are quite different from each other, which can be correlated to the number of aromatic sextet rings gained from the closed-shell to the diradical resonance forms.[7] Our group reported that a *p*-QDM-bridged heptazethrene (HZ) has an open-shell singlet diradical ground state,[4b,c] while the *m*-QDM-bridged isomer *m*-HZ has a triplet biradical ground state because no Kekulé structure can be drawn for this molecule (Figure 1b).[8] However, there are rare discussions on the physical properties and chemical reactivity of other isomers containing a higher order quinodimethane substructure. Herein, two naphthoquinodimethane isomers, the 2,6-naphthoquinodimethane (2,6-NQDM) and 1,5-naphthoquinodimethane (1,5-NQDM), will be investigated. These two molecules can be depicted as resonances of a quinoidal form and a diradical form with recovery of an aromatic naphthalene ring (Figure 1d). More informative diradical character indices y_0 of 2,6-NQDM and 1,5-NQDM were calculated (UCAM-B3LYP/6-31G(d,p) method) to be 0.01 and 0.33, respectively (y_0 is derivated from the occupation number of the lowest unoccupied natural orbital in the ground state, $0 < y_0 < 1$, 0 representing closed-shell state and 1 representing a pure diradical

Received: January 26, 2016
Published: March 11, 2016

DOI: 10.1021/acs.joc.6b00172
J. Org. Chem. 2016, 81, 2911−2919

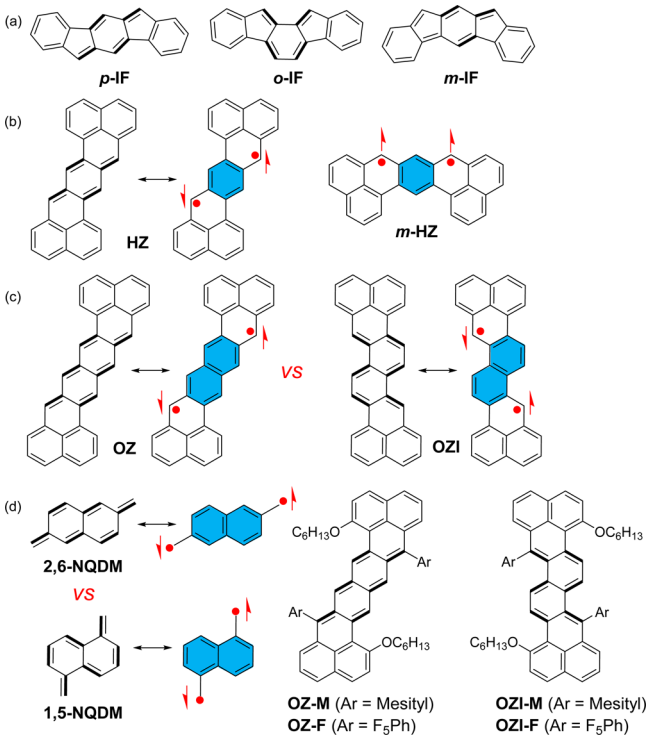

Figure 1. (a) Three indenofluorene isomers; (b) heptazethrene and its isomer; (c) octazethrene and its isomer; (d) structures of 2,6-NQDM and 1,5-NQDM and the four targeted molecules.

state). There are a few reports on the 2,6-NQDM-based singlet diradicaloids such as the extended diphenalenenoindacene,[3d] indenofluorene,[2e] and octazethrene.[4c] However, to the best of our knowledge, there is no report on the 1,5-NQDM congeners. Our particular interest here is to synthesize and study the properties of two isomers, the 2,6-NQDM-bridged octazethrene and the 1,5-NQDM bridged octazethrene (Figure 1c,d). Both isomers should have an open-shell singlet diradical ground state due to the recovery of an aromatic naphthalene ring in the diradical form, and the major difference is that the first isomer contains two fused *p*-QDM units, while the second isomer has two fused *o*-QDM units. Thus, it is interesting to study which isomer has a larger diradical character and how this difference affects their chemical reactivity and physical properties. To stabilize the reactive species, it is necessary to introduce bulky mesityl or electron-deficient pentafluorophenyl substituents to block the most reactive sites (Figure 1d). At the same time, the hexyloxy groups are attached to the two terminal naphthalene units to control the regioselective reaction and to improve the solubility.

RESULTS AND DISCUSSION

Synthesis. Previously, we reported that the triisopropylsilyl ethynyl (TIPS)-substituted octazethrene analogue **OZ-TIPS** could be synthesized via a two-step route which involves a nucleophilic addition of the diketone precursor with organolithium regent, followed by reduction with $SnCl_2$.[4c] However, there are some limitations of this method: (1) the synthesis and purification of the octazethrene diketone intermediate is tedious and the yield is very low; (2) due to the poor solubility of the octazethrene diketone intermediate, the yield of the addition step is low; and (3) it is hard to introduce other substituents (e.g., aryl) to the bay region due to the undesirable Michael addition side reaction. Herein, we report a much more efficient alternative method to synthesize the mesityl and pentafluorophenyl substituted octazethrene derivatives (**OZ-M** and **OZ-F**, respectively), and a similar strategy can be applied to the synthesis of the octazethrene isomers (**OZI-M** and **OZI-F**) (Scheme 1). The key building blocks are the naphthalene derivatives **4** and **11** carrying two triflate and two aldehyde groups at different positions. The synthesis commenced from the protection of the hydroxyl group of 3,7-dibromonaphthalene-2,6-diol **1** by MOM group to give **2** in 90% yield. Compound **2** was treated with *n*-BuLi followed by addition of anhydrous DMF to afford the dialdehyde **3** in 65% yield. The key building block compound **4** was then obtained in 85% overall yield by removal of MOM protective groups in **3** followed by reaction with trifluoromethanesulfonic anhydride. Suzuki coupling reaction between **4** and (2-(hexyloxy)naphthalen-1-yl)boronic acid **9** afforded **5** in 90% yield. The alkoxy chain was introduced to improve the solubility and prevent the formation of a five-membered ring containing isomer. Then, compound **5** was treated with mesitylmagnesium bromide or pentafluorophenylmagnesium bromide to give the corresponding diol **6a** or **6b**, which was subjected to a $BF_3{\cdot}OEt_2$-mediated Friedel–Crafts alkylation reaction to give the dihydro precursor **7a** or **7b**. Compounds **OZ-M** and **OZ-F** were finally obtained as black solids by oxidative dehydrogenation of **7a**/**7b** with DDQ. The synthesis of the octazethrene isomer dihydro-precursors **14a**/**14b** followed a strategy similar to that for the synthesis of **7a**/**7b** but starting from the 1,5-dibromonaphthalene-2,6-diol **8** (Scheme 1). The dehydrogenation of precursor **14a** was conducted by treatment with DDQ in dry toluene at room temperature. However, this gave a quite reactive species (**OZI-M**), which was transformed into the dioxo compound **15** (dark red solid) over 1 h. Workup and purification in air afforded compound **15** in 35% yield. However, the pentafluorophenyl-substituted precursor **14b** cannot be dehydrogenated by DDQ even under reflux in toluene. The structures of compounds **OZ-M**, **OZ-F**, and **15** were unambiguously identified by NMR, high-resolution mass spectrometry, and X-ray crystallographic analysis (vide infra and SI).

Ground States of OZ-M and OZ-F. Compounds **OZ-M** and **OZ-F** were experimentally identified to have an open-shell singlet diradical ground state by magnetic measurements. The solutions of **OZ-M** and **OZ-F** in toluene-d_8 show broadened NMR signals at high temperature, and the spectra become sharper at lower temperature (Figure S1, SI), which is a typical phenomenon for the singlet diradicaloids. The powders of **OZ-M** and **OZ-F** exhibit a broad electron spin resonance (ESR) spectrum at $g_e = 2.0027$ and $g_e = 2.0029$, respectively (Figure 2a, c), and the signal intensity decreases as the temperature decreases, again implying a singlet ground state for both compounds. The superconducting quantum interference device (SQUID) measurements further confirmed their singlet ground states as the magnetic susceptibility increases with increase of temperature after 250 K, correlating to a thermal population from singlet to paramagnetic triplet state (Figure 2b, d). The singlet–triplet energy gap ($\Delta E_{S\text{-}T}$) was estimated to be −1915.7 K (−3.81 kcal/mol) for **OZ-M** and −1980 K (−3.93 kcal/mol) for compound **OZ-F** by a careful fitting of the data using the Bleaney–Bowers equation.[10]

Single crystals suitable for X-ray crystallographic analysis were obtained for **OZ-M** and **OZ-F** by the solvent diffusion method, and their structures are shown in Figure 3.[11] Both molecules are slightly deviated from planarity due to the steric hindrance

DOI: 10.1021/acs.joc.6b00172
J. Org. Chem. 2016, 81, 2911–2919

Scheme 1[a]

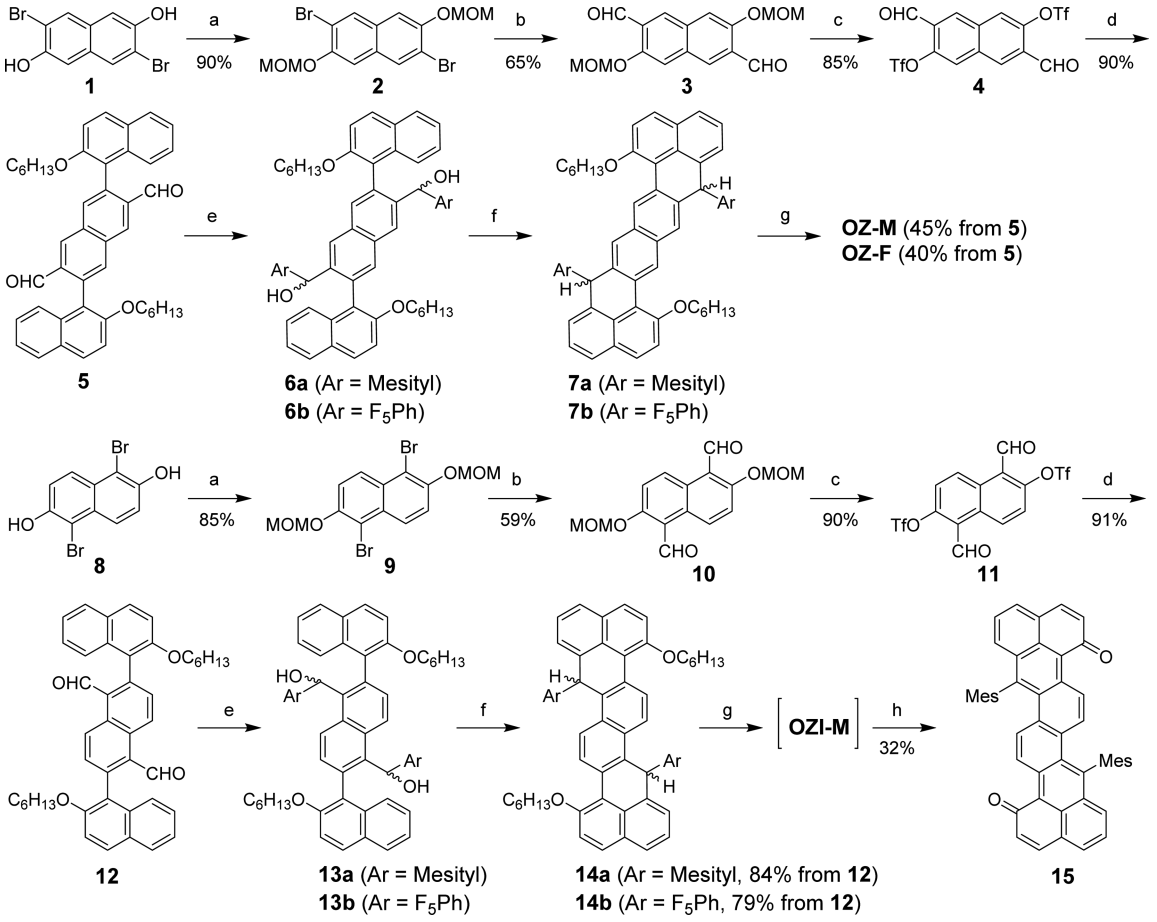

[a]Reagents and conditions: (a) NaH, MOMCl, THF, 0 °C to rt; (b) *n*-BuLi, dry THF, DMF, −78 °C to rt; (c) (1) concd HCl, dry THF, 50 °C, (2) $(OTf)_2O$, pyridine, dry DCM, 0 °C; (d) (2-(hexyloxy)naphthalen-1-yl)boronic acid, $Pd(PPh_3)_4$, 2 M K_2CO_3, toluene/H_2O/ethanol, reflux; (e) ArMgBr, Ar = mesityl or pentafluorophenyl, dry THF; (f) $BF_3{\cdot}OEt_2$, dry DCM, rt; (g) DDQ, dry toluene, rt for **OZ-M** and **OZI-M**, 45 °C for **OZ-F**; (h) workup in air. MOMCl: chloromethyl methyl ether; DDQ: 2,3-dichloro-5,6-dicyano-1,4-benzoquinone; $(OTf)_2O$: trifluoromethanesulfonic anhydride.

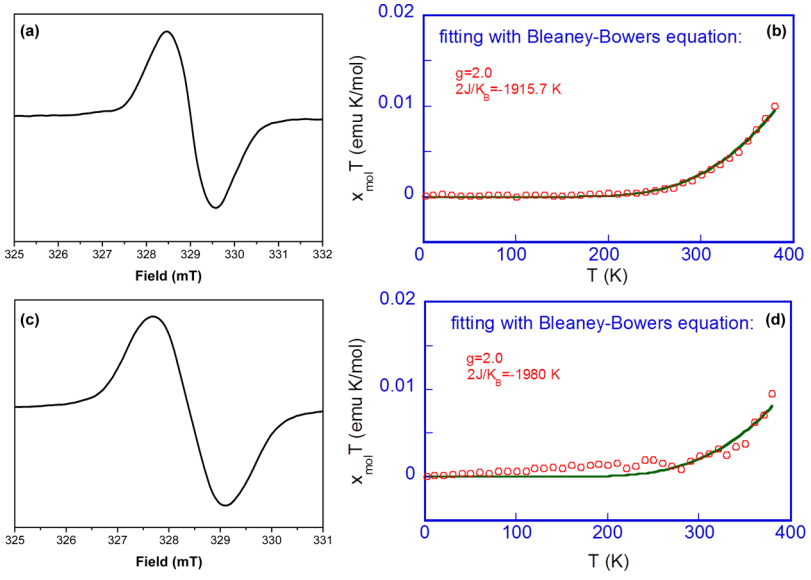

Figure 2. (Left) ESR spectrum of compounds (a) **OZ-M** and (c) **OZ-F** in powder measured at room temperature. (Right) $\chi T - T$ plot for the solid samples of (b) **OZ-M** and (d) **OZ-F** in SQUID measurements. The measured data were plotted as open circles, and the fitting curve was drawn using the Bleaney−Bowers equation with $g_e = 2.00$.

DOI: 10.1021/acs.joc.6b00172
J. Org. Chem. 2016, 81, 2911−2919

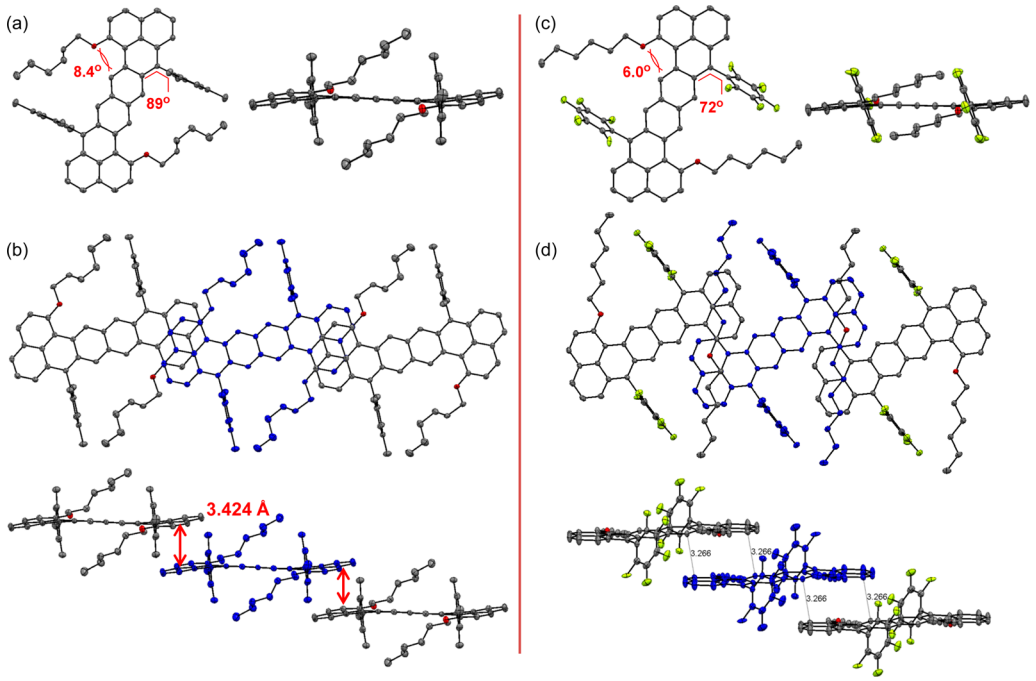

Figure 3. ORTEP drawings of the single-crystal structures of (a) **OZ-M** and (c) **OZ-F** and (b, d) their 3D packing structures, each with a top view and a side view. Solvent molecules and hydrogen atoms are omitted for clarity.

between the aryl/alkoxyl groups and the main π-conjugated framework, with a torsional angle of 8.4° for **OZ-M** and 6.0° for **OZ-F**. The mesityl and the pentafluorophenyl groups are nearly perpendicular to the octazethrene backbone, with a dihedral angle of 89° and 72°, respectively (Figure 3a,c). Both molecules are packed into a one-dimensional polymeric chain structure via intermolecular $\pi-\pi$ (or spin−spin) interactions (Figure 3b,d). Significant π-surface overlap was observed in **OZ-M**, with an average π-stacking distance of 3.424 Å. A similar observation was found in Kubo's bis(phenalenyl) molecule with an even smaller π-stacking distance of 3.137 Å.[3e] In **OZ-F**, there is almost no overlap between the octazethrene π-surfaces, but close contacts between the edge carbon atoms with a short distance of 3.266 Å was observed, which may imply moderate intermolecular spin−spin interactions.

Both **OZ-M** and **OZ-F** exhibit obvious bond alternation in the central 2,6-NQDM framework (Figure 4a and Figure S2, SI). However, the exomethylene double bonds (bond *a*) in **OZ-M** (1.388 Å) and **OZ-F** (1.392 Å) are much longer than the double bond in olefins (1.33−1.34 Å), indicating remarkable contribution of the diradical resonance form to the ground state electronic structure. The calculated nucleus-independent chemical shift (NICS(1)zz)[12] values of molecule **OZ-M** displayed remarkable aromatic character for the central benzene ring A (−11.2 ppm) and two terminal naphthalene units (rings C: −20.4 ppm and ring D: −15.2 ppm), indicating a great contribution from the diradical resonance form. NICS(1)zz calculations of molecule **OZ-F** show similar results, with −10.4, −20.5, and −15.2 ppm, for rings A, C, and D, respectively. Broken symmetry DFT calculations (UCAM-B3LYP/6-31G(d,p)) also predict that the energy of the singlet biradical (SB) state is 5.8 and 9.4 kcal/mol lower than that of the triplet biradical (TB) and closed-shell (CS) states, respectively, for **OZ-M**, while the energy of the SB state is 5.7 and 10.8 kcal/mol lower than those of the TB and CS states, respectively, for **OZ-F**. Therefore, both molecules feature a singlet diradical ground state. Diradical

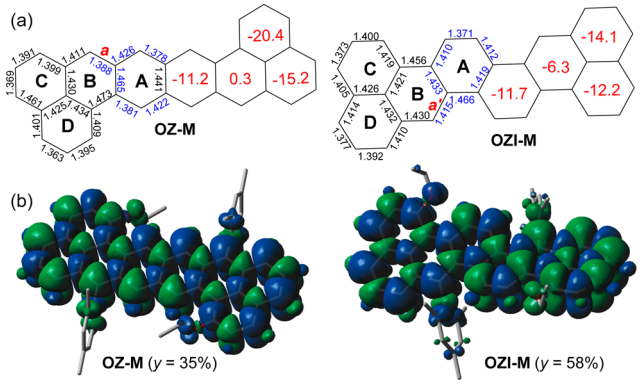

Figure 4. (a) Mean values of bond length (Å) (from crystallographic structure for **OZ-M** and from calculation for **OZI-M**) and calculated NICS(1)zz values (red numbers in the hexagons) in the molecular backbone. (b) Calculated (UCAM-B3LYP) spin density distribution of the singlet diradicals of **OZ-M** and **OZI-M**. To simplify the calculations, the hexyloxy group is replaced by the ethoxy group.

character index y_0 of **OZ-M** and **OZ-F** was calculated to be 0.35 and 0.34, respectively. These theoretical calculations are in good agreement with the magnetic observations. In accord with the moderate diradical character, the calculated singly occupied molecular orbital (SOMO) profiles of the α and β spin of both molecules showed disjoint feature (Figure S3, SI). The spin densities are evenly distributed throughout the whole octazethrene framework and even to the mesityl and pentafluorophenyl substituents (Figure 4b), explaining the good stabilities of both compounds. For comparison, **OZ-TIPS** was calculated to have a larger diradical character (y_0 = 0.434) and smaller singlet−triplet energy gap (ΔE_{S-T} = −4.4 kcal/mol) due to more effective conjugation between the TIPS groups and the octazethrene framework.[4c]

Ground State of OZI-M. As can be seen from Figure 1, molecule **OZI-M** could show significant diradical character due

DOI: 10.1021/acs.joc.6b00172
J. Org. Chem. 2016, 81, 2911−2919

to the recovery of the central aromatic naphthalene ring, similar to that of **OZ-M**. DFT calculations (UCAM-B3LYP/6-31G(d,p)) show that the energy of its SB state is 2.1 and 11.8 kcal/mol lower than the TB and closed-shell states, thus also identifying an open-shell singlet ground state. However, the calculated ΔE_{S-T} value (−2.1 kcal/mol) of **OZI-M** is much smaller than those for **OZ-M** and **OZ-F**; as a result, **OZI-M** has a much larger diradical character (y_0 = 0.58). The calculated SOMO profiles of the α and β spin of **OZI-M** showed similar disjoint feature, and the spin densities are distributed throughout the entire π-conjugated backbone (Figure 4b and Figure S3, SI). Because of the existence of steric repulsion between the mesityl and alkoxy substituents with the central naphthalene unit, the calculated geometry of **OZI-M** displays a twisted structure (Figure 4b and Figure S3, SI). Bond length analysis on the central 1,5-NQDM unit in **OZI-M** shows that the extra methylene double bond (bond a') is much longer (1.415 Å) than the bond a in **OZ-M**, implying a larger diradical character (Figure 4a). The NICS(1)zz values of **OZI-M** display comparable aromatic character for the central benzene ring (ring A, −11.7 ppm) and two terminal naphthalene units (ring C, −12.2, and ring D, −14.1 ppm). The bridging ring B shows a negative NICS(1)zz value (−6.3 ppm), while the corresponding ring B in **OZ-M** has a near-zero NICS(1)zz value (0.3 ppm), again indicating that **OZI-M** has a larger contribution of the diradical resonance form. The larger diradical character and the existence of larger strain in **OZI-M** make it more reactive than **OZ-M**, as we observed experimentally. Indeed, the in situ generated **OZI-M** is highly reactive, and only the dioxo product **15** was isolated, which was identified by X-ray crystallographic analysis.[13] Molecule **15** has a twisted structure with a large torsional angle of 18.3°, and bond length analysis reveals a fused anthracene dimer structure annulated with two α,β-unsaturated ketone units (Figure 5).

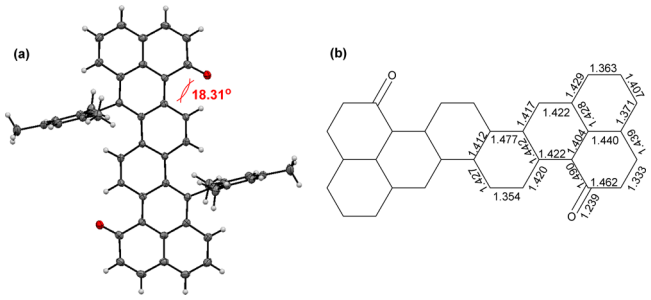

Figure 5. (a) ORTEP drawing of the crystallographic structure of **15**; (b) mean bond lengths (Å) of the backbone.

Compared to the desired compound **OZI-M**, the hexyl groups are kicked off and two ketone groups are formed with recovery of two fused anthracene rings. This unusual reaction could be explained by the large spin density (0.23) at the carbon atoms linked with the hexyloxy chains (Figure S4, SI). The **OZI-M** is so reactive that it cannot be directly determined by in situ ESR measurement during the dehydrogenation reaction. An intense single-line ESR signal (g_e = 2.00273) was observed after addition of the DDQ over 15 min (Figure S5, SI), and the spin concentration was determined to be about 63.5% by using DPPH as standard under the same concentration and the same measurement conditions. The variable-temperature (VT) ESR measurements on the solid sample after removal of the solvent under nitrogen showed that the ESR intensity (I) increased with decreasing temperature (T), with I being approximately proportional to $1/T$ (Figure S5, SI), indicating that the major magnetically active species in the mixture is a monoradical intermediate rather than the diradical, which may be due to the high reactivity and the short lifetime of **OZI-M**.

Optical and Electrochemical Properties. Compound **OZ-M** in dichloromethane (DCM) solution displays a well-resolved spectrum in the UV−vis−NIR region with an intense absorption at 649 nm ($\varepsilon = 8.7 \times 10^4$ M^{-1} cm^{-1}) and two weak bands at 692 and 757 nm (Figure 6a and Table 1). The band shape is similar to

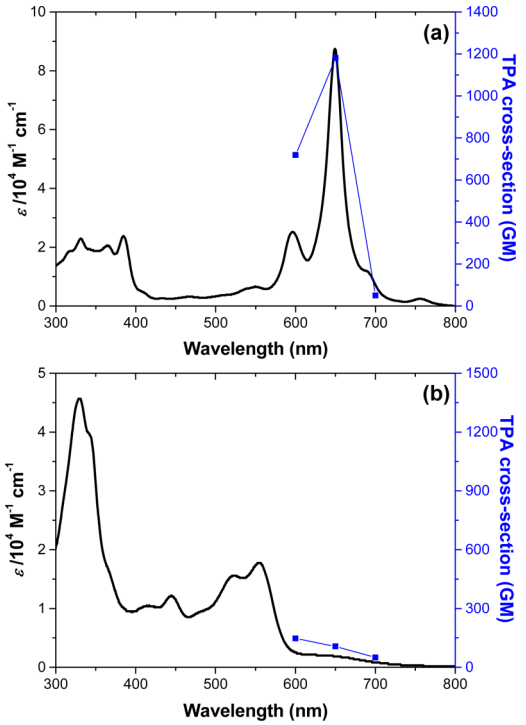

Figure 6. One-photon and two-photon absorption spectra of (a) **OZ-M** and (b) **15** recorded in toluene. TPA spectra are plotted at $\lambda_{ex}/2$.

those for many reported diradicaloids,[4−6] and the weak absorption bands in the low-energy region originate from the presence of a low-lying singlet excited state dominated by a doubly excited electronic configuration (H,H → L,L).[14] Compound **OZ-F** with a different substituent group at the bay region shows almost the same absorption spectrum as that of **OZ-M** (Figure S6, SI). However, compared with the **OZ-TIPS**,[4b] the lowest energy absorption maximum of **OZ-M** or **OZ-F** is blue-shifted about 38 nm due to the less effective conjugation between the octazethrene backbone and the mesityl/phenyl substituents. Compound **15** exhibits a very different absorption spectrum, with a broad band between 450 and 600 nm and a weak absorption tail up to 750 nm (Figure 6b and Table 1). This long absorption tail might be affected by the intramolecular charge transfer due to the existence of two ketone groups.

The excited-state dynamics of compounds **OZ-M**, **OZ-F**, and **15** were investigated by femtosecond transient absorption (TA) measurements. Compounds **OZ-M** and **OZ-F** exhibit similar TA spectra with a ground-state bleaching (GSB) signal around 650 nm as well as two weak excited-state absorption (ESA) bands in the 450−550 and 700−850 nm spectral regions (Figure 7a and Figure S7, SI). The singlet excited-state lifetimes (τ) of **OZ-M** and **OZ-F** were determined to be 2.3 and 2.4 ns, respectively, which are slightly longer than that of **OZ-TIPS** (τ = 1.6 ns)[4c] due

DOI: 10.1021/acs.joc.6b00172
J. Org. Chem. 2016, 81, 2911−2919

Table 1. Photophysical and Electrochemical Data of the Compounds OZ-M, OZ-F, and 15[a]

	λ_{max} (nm)	ε_{max} ($M^{-1}cm^{-1}$)	$E_{ox}^{1/2}$ (V)	$E_{red}^{1/2}$ (V)	HOMO (eV)	LUMO (eV)	E_g^{EC} (eV)	E_g^{Opt} (eV)	τ (ps)	$\sigma^{(2)}_{max}$ (GM)
OZ-M	595	25110								
	648	87420	0.30	−1.82	−4.44	−3.09	1.35	1.56	2300	1200 (1300 nm)
	692	11470	0.09							
	757	2450								
OZ-F	596	19140								
	649	63770	0.01	−1.88	−4.71	−3.37	1.34	1.58	2400	1300 (1300 nm)
	688	12230	0.28	−1.52						
	754	2130								
15	328	45780								
	445	12160		−2.32						
	519	15380	0.88	−1.54	−5.61	−3.51	2.10	1.66	1200	150 (1200 nm)
	554	17670		−1.41						

[a] λ_{max}: maximum absorption peak wavelength. ε_{max}: molar extinction coefficient at the absorption maximum. $E_{ox}^{1/2}$ and $E_{red}^{1/2}$ are half-wave potentials of the oxidative and reductive waves, respectively, with potentials versus Fc/Fc^+ couple. HOMO and LUMO energy levels were calculated according to the equations HOMO = $-(4.8 + E_{ox}^{onset})$ eV and LUMO = $-(4.8 + E_{red}^{onset})$ eV, where E_{ox}^{onset} and E_{red}^{onset} are the onset potentials of the first oxidative and reductive redox wave, respectively. E_g^{EC}: electrochemical energy gap derived from LUMO−HOMO. E_g^{Opt}: optical energy gap derived from lowest energy absorption onset in the absorption spectra. τ: excited lifetime based on the TA measurements. $\sigma^{(2)}_{max}$: maximum TPA cross section.

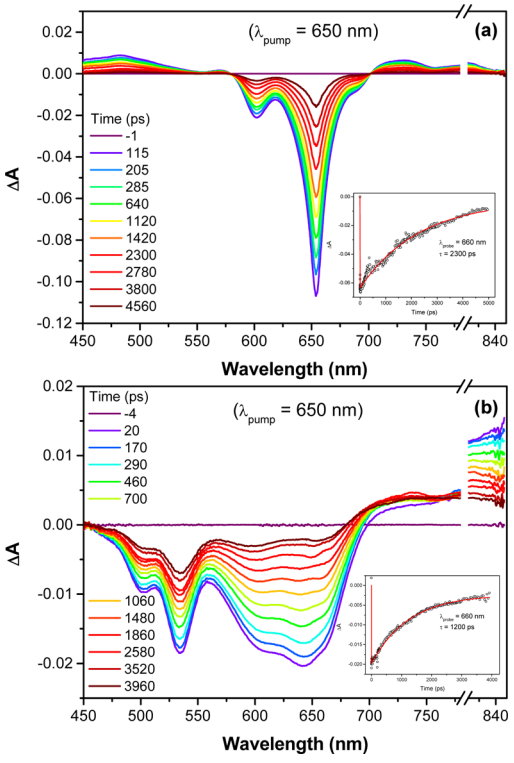

Figure 7. Femtosecond transient absorption spectra of (a) **OZ-M** and (b) **15** recorded in toluene. Insets show the decay curves.

to their smaller diradical character. The diketone compound **15** exhibits intensive GSB signal at 450−700 nm and weak ESA signal at 700−850 nm (Figure 7b). The singlet excited-state lifetime of 15 was estimated to be 1.2 ns.

Recently, many reports demonstrated that molecules with a moderate diradical character would exhibit remarkable hyperpolarizability γ.[4,7,15] Therefore, the two-photon absorption (TPA) measurements were conducted for compounds **OZ-M** and **OZ-F** by the Z-scan method (refer to the Experimental Section) in the wavelength range from 1200 to 1400 nm, where one-photon absorption contribution is negligible (Figure 6a and Figure S8, SI). Compound **OZ-M** exhibits remarkable TPA cross sections with $\sigma^{(2)}_{max}$ = 1200 GM at 1300 nm, which is slightly smaller than that of **OZ-F** ($\sigma^{(2)}_{max}$ = 1300 GM at 1300 nm) and comparable to that of **OZ-TIPS** ($\sigma^{(2)}_{max}$ = 1200 GM at 1250 nm).[4c] Compound **15** exhibits a smaller TPA cross-section ($\sigma^{(2)}_{max}$ = 150 GM at 1200 nm) in the wavelength range we measured (Figure 6b and Figure S8 in SI).

Cyclic voltammetry and differential pulse voltammetry were conducted to study the electrochemical properties of compounds **OZ-M**, **OZ-F**, and **15** (Figure 8, Table 1, and Figure S9, SI).

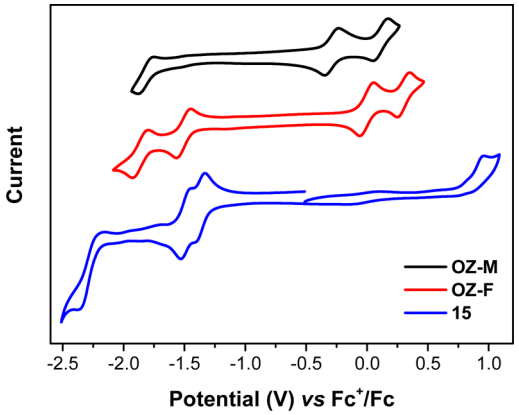

Figure 8. Cyclic voltammograms of **OZ-M**, **OZ-F**, and **15** in DCM with 0.1 M Bu_4NPF_6 as supporting electrolyte, Ag/Ag^+ as reference electrode, Au disk as working electrode, Pt wire as counter electrode, and the scan rate at 50 mV/s. The potential was externally calibrated by Fc^+/Fc couple.

Compound **OZ-M** gave two reversible oxidation waves at $E_{ox}^{1/2}$ = −0.30, 0.09 V and one quasi-reversible reduction wave at $E_{red}^{1/2}$ = −1.82 V (vs Fc/Fc^+, Fc = ferrocene), while compound **OZ-F** showed two reversible oxidation waves at $E_{ox}^{1/2}$ = −0.01, 0.28 V and two reversible reduction waves at $E_{red}^{1/2}$ = −1.52 and −1.88 V. The electrochemical energy gaps were determined as 1.35 and 1.34 eV for **OZ-M** and **OZ-F**, respectively, which are consistent with their optical energy band gap (Table 1). It is worth noting that due to the electron-withdrawing pentafluorophenyl substituents both the HOMO and LUMO of **OZ-F** are lowered in comparison to those of **OZ-M** (Table 1), leading to more

DOI: 10.1021/acs.joc.6b00172
J. Org. Chem. 2016, 81, 2911−2919

reversible reduction waves. Compound **15** showed three reduction waves with $E_{red}^{1/2}$ = −1.41, −1.54, and −2.32 V due to the electron-withdrawing character of the ketone groups, and it is difficult to oxidize.

CONCLUSIONS

In summary, we have successfully developed a new synthetic method to synthesize the 2,6-NQDM-bridged octazethrene derivatives and the 1,5-NQDM-bridged octazethrene isomers. Our detailed experimental and theoretical studies demonstrate that the bridge structure has significant effect on their diradical character and consequently on the chemical reactivity and physical properties. The amphoteric redox behavior and the ordered molecular packing of these new octazethrene derivatives make them promising candidates for ambipolar organic field-effect transistors and spin-dependent charge transport in the thin films and single crystals. The key intermediates **4** and **11** are expected to be very useful building blocks to access many quinoidal π-conjugated systems with significant diradical character. These studies are underway in our groups.

EXPERIMENTAL SECTION

General Procedures. All reagents and starting materials were obtained from commercial suppliers and used without further purification. Dry toluene and dichloromethane were distilled under a nitrogen atmosphere over sodium and calcium hydride, respectively. The precusors 3,7-dibromonaphthalene-2,6-diol (**1**) and 1,5-dibromonaphthalene-2,6-diol (**8**) (Scheme 1) and (2-(hexyloxy)naphthalen-1-yl)boronic acid were prepared according to the literature without further purification.[9,16] Column chromatography was performed on silica gel 60 (40−60 nm, 230−400 mesh). Melting points were measured on a standard melting point machine. All NMR spectra were recorded on commercial instruments (300, 500 MHz). All chemical shifts are quoted in ppm, relative to tetramethylsilane, using the residual solvent peak as a reference standard. Atmospheric pressure chemical ionization (APCI MS) was performed on a commercial mass spectrometer. MALDI-TOF mass spectra were measured on a commercial instrument using tetracyanoquinodimethane (TCNQ) as a matrix. HRMS spectra were recorded using MALDI (TOF analyzer), ESI (TOF analyzer), and EI (magnetic sector analyzer). UV−vis−NIR absorption was recorded on a commercial spectrophotometer. Cyclic voltammetry (CV) measurements were performed in dry DCM on a commerical instrument with a three-electrode cell, using 0.1 M Bu_4NPF_6 as supporting electrolyte, AgCl/Ag as reference electrode, gold disk as working electrode, Pt wire as counter electrode, and scan rate at 50 mV/s. The potential was externally calibrated against the ferrocene/ferrocenium couple. Continuous-wave X-band ESR spectra were obtained with a commercial spectrometer using a variable-temperature liquid nitrogen cryostat.

The femtosecond time-resolved transient absorption (fs-TA) spectrometer consists of an optical parametric amplifier (OPA) pumped by a Ti:sapphire regenerative amplifier system operating at 1 kHz repetition rate and an optical detection system. The generated OPA pulses have a pulse width of ∼100 fs and an average power of 1 mW in the range of 280−2700 nm, which are used as pump pulses. White light continuum (WLC) probe pulses were generated using a sapphire window (3 mm thick) by focusing a small portion of the fundamental 800 nm pulses which was picked off by a quartz plate before entering the OPA. The time delay between pump and probe beams was carefully controlled by making the pump beam travel along a variable optical delay. Intensities of the spectrally dispersed WLC probe pulses are monitored by a high speed spectrometer for both visible and near-infrared measurements. To obtain the time-resolved transient absorption difference signal (ΔA) at a specific time, the pump pulses were chopped at 500 Hz and absorption spectra intensities were saved alternately with or without pump pulse. Typically, 4000 pulses excite the samples to obtain the fs-TA spectra at each delay time. The polarization angle between pump and probe beam was set at the magic angle (54.7°) using a Glan-laser polarizer with a half-wave retarder in order to prevent polarization-dependent signals. Cross-correlation fwhm in pump−probe experiments was less than 200 fs, and the chirp of WLC probe pulses was measured to be 800 fs in the 400−800 nm region. To minimize chirp, all reflection optics in the probe beam path and a quartz cell of 2 mm path length were used. After fs-TA experiments, the absorption spectra of all compounds were carefully examined to detect if there were artifacts due to degradation and photo-oxidation of samples. The three-dimensional data sets of ΔA versus time and wavelength were subjected to singular value decomposition and global fitting to obtain the kinetic time constants and their associated spectra using Surface Xplorer software.

The two-photon absorption spectrum was measured in the NIR region using the open-aperture Z-scan method with 130 fs pulses from an optical parametric amplifier operating at a repetition rate of 1 kHz generated from a Ti:sapphire regenerative amplifier system. After passing through a 10 cm focal length lens, the laser beam was focused and passed through a 1 mm quartz cell. Since the position of the sample cell could be controlled along the laser beam direction (z axis) using the motor controlled delay stage, the local power density within the sample cell could be simply controlled under constant laser intensity. The transmitted laser beam from the sample cell was then detected by the same photodiode as used for reference monitoring. The on-axis peak intensity of the incident pulses at the focal point, I_0, ranged from 40 to 60 GW cm^{-2}. For a Gaussian beam profile, the nonlinear absorption coefficient can be obtained by curve fitting of the observed open-aperture traces $T(z)$ with eqs 1 and 2

$$T(z) = 1 - \frac{\beta I_0 (1 - e^{-\alpha_0 l})}{2\alpha_0 [1 + (z/z_0)^2]} \quad (1)$$

where α_0 is the linear absorption coefficient, l is the sample length, and z_0 is the diffraction length of the incident beam. After the nonlinear absorption coefficient has been obtained, the TPA cross section $\sigma^{(2)}$ of one solute molecule (in units of GM, where 1 GM = 10^{-50} cm^4 s photon^{-1} molecule^{-1}) can be determined by using the following relationship

$$\beta = \frac{10^{-3}\sigma^{(2)} N_A d}{h\nu} \quad (2)$$

where N_A is the Avogadro constant, d is the concentration of the compound in solution, h is the Planck constant, and ν is the frequency of the incident laser beam.

Compound 2. Compound **1** (3.17g, 10.0 mmol) was added to the NaH (0.72 g, 30.0 mmol) suspension in THF at 0 °C under argon atmosphere. The mixture was stirred for 1 h at room temperature, and chloromethyl methyl ether (2.26 mL, 30 mmol) was added. After 12 h, the mixture was quenched by water and extracted with DCM. The organic layer was dried over anhydrous $MgSO_4$. The solvent was removed under vacuum, and the residue was purified by silica gel column chromatography using DCM/hexane (1/2, v/v) as eluent to give compound **2** (3.65 g, 9.0 mmol) as a white solid in 90% yield. Mp: 148.4−150.6 °C. ^{1}H NMR ($CDCl_3$, 300 MHz): δ 7.96 (s, 2H), 7.34 (s, 2H), 5.33 (s, 4H), 3.55 (s, 6H); ^{13}C NMR ($CDCl_3$, 75 MHz): δ 150.5, 131.2, 129.8, 114.8, 110.0, 95.3, 56.3. HR-MS (EI): m/z = 403.9263, calcd for $C_{14}H_{14}Br_2O_4$ m/z = 403.9253, error = 2.47 ppm.

Compound 3. To a solution of compound **2** (2.02 g, 5.0 mmol) in dry THF (100 mL) was added dropwise n-BuLi (5 mL, 2 M) at −78 °C. The mixture was stirred for 1 h under this temperature, and then dry dimethylformamide (077 mL, 10.0 mmol) was added into the reaction mixture. After 12 h, the mixture was quenched by water and washed with water. The organic layer was extracted with DCM and dried over anhydrous $MgSO_4$. The solvent was removed under vacuum, and the residue was purified by silica gel column chromatography using DCM/hexane (2/1, v/v) as eluent to give compound **3** (0.98 g, 3.25 mmol) as a yellow solid in 65% yield. Mp: 160.0−162.1 °C. ^{1}H NMR ($CDCl_3$, 300 MHz): δ 10.16 (s, 2H), 8.29 (s, 2H), 7.59 (s, 2H), 5.39 (s, 4H), 3.56 (s, 6H); ^{13}C NMR ($CDCl_3$, 75 MHz): δ 189.8, 154.3, 131.9, 129.1, 128.0, 112.1, 95.0, 56.5. HR-MS (EI): m/z = 304.0947, calcd for $C_{16}H_{16}O_6$ m/z = 304.0941, error = 1.93 ppm.

DOI: 10.1021/acs.joc.6b00172
J. Org. Chem. 2016, 81, 2911−2919

Compound 4. To a solution of compound **3** (2.02 g, 5.0 mmol) in dry THF (50 mL) was added concentrated HCl (3.0 mL). The mixture was heated to reflux for 5 h. After the mixture was cooled to room temperature, the solvent was evaporated, and the solid was washed with water and methanol. The crude product was dissolved in 100 mL of DCM with pyridine (1.0 mL) and cooled to the 0 °C. Trifluoromethanesulfonic anhydride (10.0 mmol, 2.0 equiv) was added to the reaction mixture under this temperature, and then the mixture was allowed to warm to room temperature and stirred for further 1 h. The mixture was quenched by water and washed with 2 M HCl solution and water. The organic layer was extracted with DCM and dried over anhydrous $MgSO_4$. The solvent was removed under vacuum, and the residue was purified by silica gel column chromatography using DCM/hexane (4/1, v/v) as eluent to give compound **4** (2.04 g, 4.25 mmol) as a light yellow solid in 85% yield. Mp: 179.0−182.0 °C. ^{1}H NMR ($CDCl_3$, 300 MHz): δ 10.40 (s, 2H), 8.61 (s, 2H), 8.09 (s, 2H); ^{13}C NMR ($CDCl_3$, 75 MHz): δ 185.8 (C═O), 146.8, 133.86, 133.70, 129.6, 122.7, 120.8, 116.6. HR-MS (EI): m/z = 479.9417, calcd for $C_{14}H_6F_6O_8S_2$ m/z = 479.9403, error = 3.01 ppm.

Compound 5. A mixture of compound **4** (0.48 g, 1 mmol), (2-(hexyloxy)naphthalen-1-yl)boronic acid (0.82 g, 3 mmol), $Pd(PPh_3)_4$ (58 mg, 0.05 mmol) in toluene (25 mL), ethanol (3 mL), and K_2CO_3 aqueous solution (2 M, 3 mL) was degassed by three freeze−pump−thaw cycles. The reaction mixture was heated at 105 °C overnight under nitrogen. After being cooled to room temperature, the mixture was washed with water and extracted with DCM. The organic layer was dried over anhydrous $MgSO_4$. The solvent was removed under vacuum, and the residue was purified by silica gel column chromatography using DCM/hexane (1/1, v/v) as eluent to give compound **5** (0.57 g, 0.90 mmol) as a yellow solid in 90% yield. Mp: >350 °C. ^{1}H NMR ($CDCl_3$, 300 MHz) δ ppm: 9.82 (s, 2H), 8.68 (s, 2H), 8.11 (s, 2H), 8.01 (d, J = 9.0 Hz, 2H), 7.93−7.90 (m, 2H), 7.53−7.50 (m, 2H), 7.44−7.39 (m, 6H), 4.12−4.04 (m, 4H), 1.64−1.56(m, 4H), 1.15 (br, 12H), 0.76 (t, J = 6 Hz, 6H). ^{13}C NMR ($CDCl_3$, 75 MHz) δ ppm: 192.5 (C═O), 153.89, 153.84, 135.9, 135.0, 134.9, 134.4, 134.3, 133.9, 133.4, 129.1, 128.2, 128.1, 127.0, 124.7, 123.8, 120.0, 119.8, 114.0, 113.9, 31.2, 31.1, 29.11, 29.02, 25.3, 22.3, 13.7. HR-MS (EI): m/z = 636.3233, calcd for $C_{44}H_{44}O_4$ m/z = 636.3244, error = −0.17 ppm.

Compound OZ-M. Mesitylmagnesium (1.0 M, 1.0 mL) was added to the dry THF solution (15 mL) of compound **5** (0.06 g, 0.10 mmol) under argon atmosphere, and the mixture was stirred at room temperature for 8 h. The reaction mixture was quenched by water and extracted by chloroform. The organic layer was dried over Na_2SO_4 and the solvent was removed under reduced pressure. The crude compound **6** was then dissolved in 20 mL dry DCM under argon atmosphere and 0.2 mL of $BF_3{\cdot}OEt_2$ was added. The mixture was stirred for 5 min and quenched by methanol. The solvent was removed under reduced pressure. DDQ (0.0227 g, 0.1 mmol) was added dropwise to the 20 mL dry toluene solution of compound **7**. Upon addition of DDQ solution, the color of the reaction mixture changed slowly from light blue to dark green, and the reaction was monitored by TLC until completion. After evaporation of the solvent, the residue was purified by column chromatography (silica gel, DCM/hexane (1/3, v/v) as eluent) to give compound **OZ-M** (37 mg, 45% in three steps) as a black solid, decomposed at 217.9 °C. HR-MS (ESI): m/z = 838.4768, calcd for $C_{62}H_{62}O_2$ m/z = 838.4744, error = −2.8 ppm.

Compound OZ-F. Starting with compound **5** (60 mg, 0.10 mmol) following a procedure similar to that for compound **OZ-M** could gave compound **OZ-F** (37 mg, 0.04 mmol) as a black solid in 40% yield, decomposed at 271.5 °C. HR-MS (ESI): m/z = 935.2937, calcd for $C_{56}H_{41}F_{10}O_2$ $[M + 1]^+$ m/z = 935.2941, error =0.5 ppm.

Compound 9. Starting with 1,5-dibromonaphthalene-2,6-diol (3.17 g, 10.0 mmol) and following a procedure similar to that for compound **2**, compound **9** (3.40 g, 8.50 mmol) was obtained as a white solid in 85% yield. Mp: 102.4−103.9 °C. ^{1}H NMR ($CDCl_3$, 300 MHz): δ 8.23 (d, J = 9 Hz, 2H), 7.50 (d, J = 9 Hz, 2H), 5.35 (s, 4H), 3.57 (s, 6H); ^{13}C NMR ($CDCl_3$, 75 MHz): δ 151.0, 129.8, 127.4, 118.4, 110.4, 95.6, 56.5. HR-MS (EI): m/z = 403.9251, calcd for $C_{14}H_{14}Br_2O_4$ m/z = 403.9253, error = −0.44 ppm.

Compound 10. Starting with compound **9** (4.0 g, 10.0 mmol) and following a procedure similar to that for compound **3**, compound **10** (1.77 g, 5.9 mmol) was obtained as a yellow solid in 59% yield. Mp: 135.5−137.0 °C. ^{1}H NMR ($CDCl_3$, 300 MHz): δ 10.90 (s, 2H), 9.52 (d, J = 12 Hz, 2H), 7.59 (d, J = 12 Hz, 2H), 5.40 (s, 4H), 3.56 (s, 6H); ^{13}C NMR ($CDCl_3$, 75 MHz): δ 192.0 (C═O), 160.6, 134.1, 127.1, 118.6, 117.4, 95.1, 56.7. HR-MS (EI): m/z = 304.0946, calcd for $C_{16}H_{16}O_6$ m/z = 304.0941, error = 1.53 ppm.

Compound 11. Starting with compound **10** (1.52 g, 5.0 mmol) and following a procedure similar to that for compound **4**, compound **11** (2.16 g, 4.5 mmol) was obtained as a yellow solid in 90% yield. Mp: 128.5−130.0 °C. ^{1}H NMR ($CDCl_3$, 300 MHz): δ 10.90 (s, 2H), 9.66 (d, J = 9 Hz, 2H), 7.77 (d, J = 9 Hz, 2H); ^{13}C NMR ($CDCl_3$, 75 MHz): δ187.8 (C═O), 152.5, 134.9, 130.5, 123.9, 122.6, 120.6, 116.4. HR-MS (EI): m/z = 479.9414, calcd for $C_{14}H_6F_6O_8S_2$, m/z = 479.9403, error = 2.37 ppm.

Compound 12. Starting with compound **11** (0.48 g, 1.0 mmol) and following a procedure similar to that for compound **5**, compound **12** (0.58 g, 0.91 mmol) was obtained as a yellow solid in 91% yield. Mp: >350 °C. ^{1}H NMR ($CDCl_3$, 300 MHz): δ 10.11 (s, 2H), 9.77−9.73 (m, 2H), 7.99 (d, J = 9 Hz, 2H), 7.92−7.88 (m, 2H), 7.66 (d, J = 9 Hz, 2H), 7.41−7.32 (m, 8H), 4.13−4.04 (m, 4H), 1.62−1.58 (m, 4H), 1.21−1.14 (m, 12H), 0.79−0.74 (m, 6H); ^{13}C NMR ($CDCl_3$, 75 MHz): δ ppm 195.2 (C═O), 154.0, 153.9, 144.1, 144.0, 133.8, 133.6, 132.84, 132.80, 131.83, 131.80, 130.69, 130.65, 130.5, 129.58, 129.51, 128.9, 128.8, 128.1, 127.14, 127.10, 125.0, 124.9, 123.93, 123.90, 120.8, 120.7, 114.2, 114.1, 69.4, 69.3, 31.29, 31.21, 29.1, 29.0, 25.4, 25.3, 22.4, 22.3, 13.85, 13.80. HR-MS (EI): m/z = 636.3232, calcd for $C_{44}H_{44}O_4$ m/z = 636.3234, error = −0.34 ppm.

Compound 15. Following a procedure similar to that for compound **7**, oxidation precursor compound **14** was obtained as a yellow solid. DDQ (1 equiv) was added dropwise to the 20 mL of a dry toluene solution of compound **14** (84.1 mg, 0.10 mmol). Upon addition of DDQ solution, the color of the reaction mixture changed quickly from light yellow to dark green, and then the color changed to dark red over 1 h under argon. After evaporation of the solvent, the residue was purified by column chromatography (silica gel, hexane/ethyl acetate (4/1, v/v) as eluent) to give compound **15** (21.4 mg, 0.03 mmol) as a red-black solid in 32% yield. Mp: >350 °C. ^{1}H NMR (THF-d_8, 500 MHz): δ ppm 9.82 (d, J = 10 Hz, 2H), 8.07 (d, J = 10 Hz, 2H), 7.95 (d, J = 5 Hz, 2H), 7.86 (d, J = 10 Hz, 2H), 7.74 (d, J = 10 Hz, 2H), 7.55−7.52 (m, 2H), 7.14 (s, 4H), 6.75 (d, J = 10 Hz, 2H), 2.48 (s, 6H), 1.69 (s, 12H); ^{13}C NMR (THF-d_8, 75 MHz): δ ppm 184.9 (C═O), 143.5, 136.5, 136.4, 135.3, 134.2, 131.9, 130.5, 129.4, 128.6, 128.48, 128.40, 127.4, 127.3, 126.6, 126.5, 125.7, 124.1, 122.0, 119.7, 27.7,18.4, 17.6. HR-MS (ESI): m/z = 669.2792, calcd for $C_{50}H_{37}O_2$ $[M + 1]^+$ m/z = 669.2788, error = −0.5 ppm.

■ ASSOCIATED CONTENT

Supporting Information

X-ray crystallography (CIF files), additional physical characterization data and theoretical calculations are in Supporting Information. The Supporting Information is available free of charge on the ACS Publications website at DOI: 10.1021/acs.joc.6b00172.

Physical characterization data and theoretical calculations (PDF)

X-ray crystallographic data for **15** (CIF)

X-ray crystallographic data for **OZ-F** (CIF)

X-ray crystallographic data for **OZ-M** (CIF)

■ AUTHOR INFORMATION

Corresponding Authors

*E-mail: msedingj@nus.edu.sg.

*E-mail: dongho@yonsei.ac.kr.

*E-mail: chmwuj@nus.edu.sg.

DOI: 10.1021/acs.joc.6b00172
J. Org. Chem. 2016, 81, 2911−2919

Notes

The authors declare no competing financial interest.

■ ACKNOWLEDGMENTS

J.W. acknowledges financial support from the MOE Tier 3 Programme (MOE2014-T3-1-004), Tier 2 grant (MOE2014-T2-1-080), and A*STAR JCO grant (1431AFG100). This work at Yonsei University was supported by the Global Frontier R&D Program on Center for Multiscale Energy System funded by the National Research Foundation under the Ministry of Science, ICT & Future, Korea (NRF-2014M3A6A7060583). We thank Dr. Tan Geok Kheng and Dr. Bruno Donnadieu for the crystallographic analysis.

■ REFERENCES

(1) (a) Sun, Z.; Zeng, Z.; Wu, J. *Acc. Chem. Res.* **2014**, *47*, 2582−2591. (b) Kubo, T. *Chem. Lett.* **2015**, *44*, 111−122. (c) Zeng, Z.; Shi, X.; Chi, C.; López Navarrete, J. T.; Casado, J.; Wu, J. *Chem. Soc. Rev.* **2015**, *44*, 6578−6596.

(2) (a) Chase, D. T.; Rose, B. D.; McClintock, S. P.; Zakharov, L. N.; Haley, M. M. *Angew. Chem., Int. Ed.* **2011**, *50*, 1127−1130. (b) Shimizu, A.; Tobe, Y. *Angew. Chem., Int. Ed.* **2011**, *50*, 6906−6910. (c) Fix, A. G.; Chase, D. T.; Haley, M. M. *Top. Curr. Chem.* **2012**, *69*, 890−911. (d) Fix, A. G.; Deal, P. E.; Vonnegut, C. L.; Rose, B. D.; Zakharov, L. N.; Haley, M. M. *Org. Lett.* **2013**, *15*, 1362−1365. (e) Rose, B. D.; Vonnegut, C. L.; Zakharov, L. N.; Haley, M. M. *Org. Lett.* **2012**, *14*, 2426−2429. (f) Shimizu, A.; Kishi, R.; Nakano, M.; Shiomi, D.; Sato, K.; Takui, T.; Hisaki, I.; Miyata, M.; Tobe, Y. *Angew. Chem., Int. Ed.* **2013**, *52*, 6076−6079. (g) Miyoshi, H.; Nobusue, S.; Shimizu, A.; Hisaki, I.; Miyata, M.; Tobe, Y. *Chem. Sci.* **2014**, *5*, 163−168. (h) Young, B. S.; Chase, D. T.; Marshall, J. L.; Vonnegut, C. L.; Zakharov, L. N.; Haley, M. M. *Chem. Sci.* **2014**, *5*, 1008−1014. (i) Shimizu, A.; Nobusue, S.; Miyoshi, H.; Tobe, Y. *Pure Appl. Chem.* **2014**, *86*, 517−528.

(3) (a) Ohashi, K.; Kubo, T.; Masui, T.; Yamamoto, K.; Nakasuji, K.; Takui, T.; Kai, Y.; Murata, I. *J. Am. Chem. Soc.* **1998**, *120*, 2018−2027. (b) Kubo, T.; Sakamoto, M.; Akabane, M.; Fujiwara, Y.; Yamamoto, K.; Akita, M.; Inoue, K.; Takui, T.; Nakasuji, K. *Angew. Chem., Int. Ed.* **2004**, *43*, 6474−6479. (c) Kubo, T.; Shimizu, A.; Sakamoto, M.; Uruichi, M.; Yakushi, K.; Nakano, M.; Shiomi, D.; Sato, K.; Takui, T.; Morita, Y.; Nakasuji, K. *Angew. Chem., Int. Ed.* **2005**, *44*, 6564−6568. (d) Kubo, T.; Shimizu, A.; Uruichi, M.; Yakushi, K.; Nakano, M.; Shiomi, D.; Sato, K.; Takui, T.; Morita, Y.; Nakasuji, K. *Org. Lett.* **2007**, *9*, 81−84. (e) Shimizu, A.; Uruichi, M.; Yakushi, K.; Matsuzaki, H.; Okamoto, H.; Nakano, M.; Hirao, Y.; Matsumoto, K.; Kurata, H.; Kubo, T. *Angew. Chem., Int. Ed.* **2009**, *48*, 5482−5486. (f) Shimizu, A.; Kubo, T.; Uruichi, M.; Yakushi, K.; Nakano, M.; Shiomi, D.; Sato, K.; Takui, T.; Hirao, Y.; Matsumoto, K.; Kurata, H.; Morita, Y.; Nakasuji, K. *J. Am. Chem. Soc.* **2010**, *132*, 14421−14428. (g) Shimizu, A.; Hirao, Y.; Matsumoto, K.; Kurata, H.; Kubo, T.; Uruichi, M.; Yakushi, K. *Chem. Commun.* **2012**, *48*, 5629−5631.

(4) (a) Umeda, R.; Hibi, D.; Miki, K.; Tobe, Y. *Org. Lett.* **2009**, *11*, 4104−4106. (b) Sun, Z.; Huang, K.-W.; Wu, J. *J. Am. Chem. Soc.* **2011**, *133*, 11896−11899. (c) Li, Y.; Heng, K.-W.; Lee, B. S.; Aratani, N.; Zafra, J. L.; Bao, N.; Lee, R.; Sung, Y. M.; Sun, Z.; Huang, K.-W.; Webster, R. D.; López Navarrete, J. T.; Kim, D.; Osuka, A.; Casado, J.; Ding, J.; Wu, J. *J. Am. Chem. Soc.* **2012**, *134*, 14913−14922. (d) Hu, P.; Lee, S.; Herng, T. S.; Aratani, N.; Gonçalves, T. P.; Qi, Q.; Shi, X.; Yamada, H.; Huang, K.-W.; Ding, J.; Kim, D.; Wu, J. *J. Am. Chem. Soc.* **2016**, *138*, 1065−1077. (e) Ni, Y.; Lee, S.; Son, M.; Aratani, N.; Ishida, M.; Samanta, A.; Yamada, H.; Chang, Y.-T.; Furuta, H.; Kim, D.; Wu, J. *Angew. Chem., Int. Ed.* **2016**, *55*, 2815−2819.

(5) (a) Konishi, A.; Hirao, Y.; Nakano, M.; Shimizu, A.; Botek, E.; Champagne, B.; Shiomi, D.; Sato, K.; Takui, T.; Matsumoto, K.; Kurata, H.; Kubo, T. *J. Am. Chem. Soc.* **2010**, *132*, 11021−11023. (b) Konishi, A.; Hirao, Y.; Matsumoto, K.; Kurata, H.; Kishi, R.; Shigeta, Y.; Nakano, M.; Tokunaga, K.; Kamada, K.; Kubo, T. *J. Am. Chem. Soc.* **2013**, *135*, 1430−1437.

(6) (a) Zeng, Z.; Ishida, M.; Zafra, J. L.; Zhu, X.; Sung, Y. M.; Bao, N.; Webster, R. D.; Lee, B. S.; Li, R.-W.; Zeng, W.; Li, Y.; Chi, C.; López Navarrete, J. T.; Ding, J.; Casado, J.; Kim, D.; Wu, J. *J. Am. Chem. Soc.* **2013**, *135*, 6363−6371. (b) Zeng, Z.; Lee, S.; Zafra, J. L.; Ishida, M.; Zhu, X.; Sun, Z.; Ni, Y.; Webster, R. D.; Li, R.-W.; López Navarrete, J. T.; Chi, C.; Ding, J.; Casado, J.; Kim, D.; Wu, J. *Angew. Chem., Int. Ed.* **2013**, *52*, 8561−8565. (c) Zeng, Z.; Lee, S.; Son, M.; Fukuda, K.; Burrezo, P. M.; Zhu, X.; Qi, Q.; Li, R.-W.; López Navarrete, J. T.; Ding, J.; Casado, J.; Nakano, M.; Kim, D.; Wu, J. *J. Am. Chem. Soc.* **2015**, *137*, 8572−8583.

(7) Luo, D.; Lee, S.; Zheng, B.; Sun, Z.; Zeng, W.; Huang, K.-W.; Furukawa, K.; Kim, D.; Webster, R. D.; Wu, J. *Chem. Sci.* **2014**, *5*, 4944−4952.

(8) Li, Y.; Huang, K.-W.; Sun, Z.; Webster, R. D.; Zeng, Z.; Zeng, W.; Chi, C.; Furukawa, K.; Wu, J. *Chem. Sci.* **2014**, *5*, 1908−1914.

(9) Cammidge, A. N.; Goddard, H. M.; Schubert, P. J.; Gopee, H.; Hughes, D. L.; Gonzalez-Lucas, D. *Org. Lett.* **2011**, *13*, 6034−6037.

(10) Bleaney, B.; Bowers, K. D. *Proc. R. Soc. London, Ser. A* **1952**, *214*, 451−453.

(11) Crystallographic data for **OZ-M**: $C_{62}H_{62}O_2$, M_w = 838.47; monoclinic; space group $P2(1)/c$; a = 8.3105(3) Å, b = 9.6129(3)Å, c = 28.8543(10) Å, α = 90°, β = 96.657(2)°, γ = 90°; V = 2289.57(14) Å^3; Z = 4; ρ_{calcd} = 1.217 Mg/m^3; R_1 = 0.0464 ($I > 2\sigma(I)$), wR_2 = 0.1148 (all data). CCDC no.: 1418608. Crystallographic data for **OZ-F**: $C_{63}H_{48}F_{10}O_2$, M_w = 1027.01; triclinic; space group P-1; a = 9.2006(4) Å, b = 10.9573(6) Å, c = 13.7554(6) Å, α = 95.316(2)°, β = 99.2040(10)°, γ = 114.8070(10)°; V = 1222.66(10) Å^3; Z = 1; ρ_{calcd} = 1.395 Mg/m^3; R_1 = 0.0529 ($I > 2\sigma(I)$), wR_2 = 0.1467 (all data). CCDC no. 1419168.

(12) Fallah-Bagher-Shaidaei, H.; Wannere, C. S.; Corminboeuf, C.; Puchta, R.; Schleyer, P. v. R. *Org. Lett.* **2006**, *8*, 863−866.

(13) Crystallographic data for **15**: $C_{50}H_{36}O_2$, M_w = 669.28; monoclinic; space group $P21/n$; a = 11.2442(6) Å, b = 12.6155(7) Å, c = 11.9818(7) Å, α = 90°, β = 92.599(3)°, γ = 90°; V = 1697.88(16) Å^3; Z = 4; ρ_{calcd} = 1.308 Mg/m^3; R_1 = 0.0413 ($I > 2\sigma(I)$), wR_2 = 0.1300 (all data). CCDC no. 1419168.

(14) Di Motta, S.; Negri, F.; Fazzi, D.; Castiglioni, C.; Canesi, E. V. *J. Phys. Chem. Lett.* **2010**, *1*, 3334−3339.

(15) (a) Nakano, M.; Nagao, H.; Yamaguchi, K. *Phys. Rev. A: At., Mol., Opt. Phys.* **1997**, *55*, 1503−1513. (b) Nakano, M.; Kishi, R.; Nitta, T.; Kubo, T.; Nakasuji, K.; Kamada, K.; Ohta, K.; Champagne, B.; Botek, E.; Yamaguchi, K. *J. Phys. Chem. A* **2005**, *109*, 885−891. (c) Nakano, M.; Kubo, T.; Kamada, K.; Ohta, K.; Kishi, R.; Ohta, S.; Nakagawa, N.; Takahashi, H.; Furukawa, S.; Morita, Y.; Nakasuji, K.; Yamaguchi, K. *Chem. Phys. Lett.* **2006**, *418*, 142. (d) Ohta, S.; Nakano, M.; Kubo, K.; Kamada, K.; Ohta, K.; Kishi, R.; Nakagawa, N.; Champagne, B.; Botek, E.; Takebe, A.; Umezaki, S.; Nate, M.; Takahashi, H.; Furukawa, S.; Morita, Y.; Nakasuji, K.; Yamaguchi, K. *J. Phys. Chem. A* **2007**, *111*, 3633−3641. (e) Champagne, B.; Nakano, M.; Kishi, R.; Takebe, A.; Nate, M.; Takahashi, H.; Kubo, T.; Kamada, K.; Ohta, K.; Botek, E. *Comput. Lett.* **2007**, *3*, 333−338. (f) Kamada, K.; Ohta, K.; Kubo, T.; Shimizu, A.; Morita, Y.; Nakasuji, K.; Kishi, R.; Ohta, S.; Furukawa, S. I.; Takahashi, H.; Nakano, M. *Angew. Chem., Int. Ed.* **2007**, *46*, 3544−3546. (g) Nakano, M.; Kishi, R.; Ohta, S.; Takahashi, H.; Kubo, T.; Kamada, K.; Ohta, K.; Botek, E.; Champagne, B. *Phys. Rev. Lett.* **2007**, *99*, 033001−033004.

(16) Osaka, I.; Shinamura, S.; Abe, T.; Takimiya, K. *J. Mater. Chem. C* **2013**, *1*, 1297−1304.

DOI: 10.1021/acs.joc.6b00172
J. Org. Chem. 2016, 81, 2911−2919